Characterization of Subunit Structural Changes Accompanying Assembly of the Bacteriophage P22 Procapsid†

Roman Tuma,‡,§ Hiro Tsuruta,‡,|| James M. Benevides,⊥ Peter E. Prevelige, Jr.,*,‡ and George J. Thomas, Jr.*,⊥

Department of Microbiology, University of Alabama at Birmingham, Birmingham, Alabama 35205, and School of Biological Sciences, University of Missouri−Kansas City, Kansas City, Missouri 64110

Received August 17, 2000; Revised Manuscript Received November 16, 2000

ABSTRACT: P22 serves as a model for the assembly and maturation of icosahedral double-stranded DNA viruses. The viral capsid precursor, or *procapsid*, is assembled from 420 copies of a 47 kDa coat protein subunit (gp5) that is rich in β-strand secondary structure. Maturation to the *capsid*, which occurs in vivo upon DNA packaging, is accompanied by shell expansion and a large increase in the level of protection against deuterium exchange of amide NH groups. Accordingly, shell maturation resembles the final step in protein folding, wherein domain packing and an exchange-protected core become more fully developed [Tuma, R., Prevelige, P. E., Jr., and Thomas, G. J., Jr. (1998) *Proc. Natl. Acad. Sci. U.S.A. 95*, 9885−9890]. Here, we exploit recent advances in Raman spectroscopy to investigate the P22 coat protein subunit under conditions which stabilize the *monomeric* state, viz., in solution at very low concentrations. Under these conditions, the monomer exhibits an elongated shape, as demonstrated by small-angle X-ray scattering. Raman spectra allow the identification of conformation-sensitive marker bands of the monomer, as well as the characterization of NH exchange dynamics for comparison with procapsid and capsid shell assemblies. We show that procapsid assembly involves significant ordering of the predominantly β-strand backbone. We propose that such ordering may mediate formation of the distinct subunit conformations required for assembly of a $T = 7$ icosahedral lattice. However, the monomer, like the subunit within the procapsid lattice, exhibits a moderate level of protection against low-temperature NH exchange, indicative of a nascent folding core. The environments and exchange characteristics of key side chains are also similar for the monomeric and procapsid subunits, and distinct from corresponding characteristics of the capsid subunit. The monomer thus represents a compact but metastable folding intermediate along the pathway to assembly of the procapsid and capsid.

Cellular functions are often performed by large macromolecular complexes, the assembly of which may involve a complex series of protein recognition events and conformational changes. Viruses serve as useful models for investigating the molecular mechanisms underlying such assembly processes. For example, the life cycle of a virus typically requires the intracellular assembly of a *capsid* from multiple copies of a few types of protein subunits. Constructing a topologically closed capsid from chemically identical or similar protein subunits requires switching between different conformations in a specific path-dependent manner (*1*). In the case of icosahedral double-stranded (ds)[1] DNA phages, the process involves the initial formation of a metastable precursor, or *procapsid*, which subsequently matures irreversibly to the stable capsid (*2*). Such a two-step mechanism, characterized by weaker intersubunit interactions in the procapsid state, may facilitate the correction of assembly errors prior to capsid maturation, stabilization, and genome packaging. Conversely, the greater stability of the mature capsid more effectively protects the viral genome from environmental insult.

Irreversible conformational changes in the capsid lattice are not limited to dsDNA bacteriophages. Recently, similar conformational changes have been observed for an insect RNA virus (*3*). Irreversible transitions also accompany proteolytic maturations in other RNA viruses (*4*). Picornaviruses employ such conformational changes to initiate disassembly and genome release upon infection (*5*−*7*). In many cases, conformational change is triggered by receptor binding or internalization (*8*). Understanding how this type of controlled plasticity can be programmed into the protein subunits of a capsid shell or precursor requires knowledge

† Supported by NIH Grant GM50776 (to G.J.T.) and NSF Grant DBI 9726698 (to P.E.P.). The SSRL facility is supported in part by the NIH NCRR (Grant RR-01209) and the DOE OBER.

* To whom correspondence may be addressed. P.E.P.: e-mail, prevelig@uab.edu; phone, (205) 975-5327; fax, (205) 975-5479. G.J.T.: e-mail, thomasgj@umkc.edu; phone, (816) 235-5247; fax, (816) 235-1503.

‡ University of Alabama at Birmingham.

§ Present address: Department of Biosciences, University of Helsinki, 00014 Helsinki, Finland.

|| Present address: Stanford Synchrotron Radiation Laboratory, MS 69, Palo Alto, CA 94309.

⊥ University of Missouri−Kansas City.

[1] Abbreviations: GuHCl, guanidinium hydrochloride; EDTA, ethylenediaminetetraacetic acid; SAXS, small-angle X-ray scattering; Tris, tris(hydroxymethyl)aminomethane; ds, double-stranded; H/D exchange, hydrogen/deuterium exchange; CD, circular dichroism; gp5, coat protein subunit of the P22 shell, encoded by viral gene 5; CCMV, cowpea chlorotic mottle virus; *T*, icosahedral triangulation number.

10.1021/bi001965y CCC: $20.00
Published on Web 12/22/2000

of the molecular structure and stability at various stages of the assembly and maturation pathway.

High-resolution structures of viruses reveal conformational switching of chemically identical subunits to accommodate different quasi-equivalent contacts within the icosahedral lattice (*9*). Although high-resolution structures unveil the different subunit conformations in great detail, in most cases they do not address the conformation of the unassembled subunit. Therefore, the mechanism by which subunits attain their final conformation remains elusive. In particular, there are two fundamentally different models of conformational switching. In one case, the discrete conformations observed in the viral shell also exist in solution, and their proportion determines the outcome of the assembly process. This mechanism has been proposed in the assembly of bacteriophage HK97 (*10*), wherein the subunits equilibrate between pentamers and hexamers, which then assemble into a $T = 7$ capsid. In the second case, unassembled subunits attain an average conformation that is distinct from any of the states observed within the viral shell assembly. Here, the final conformation is attained only upon assembly, in a manner analogous to the conventional pathway of protein folding (*11*, *12*). Such a mechanism most likely governs the morphogenesis of the RNA phage MS2 (*13*, *14*) and dsDNA phage PRD1 (*11*).

In this study, we employ a well-characterized icosahedral dsDNA virus, the *Salmonella* bacteriophage P22, to study structural changes in the coat protein subunit accompanying procapsid assembly. The assembly pathway of P22 is an established prototype for the morphogenesis of many dsDNA viruses, including the herpesviruses and adenoviruses. In each case, assembly proceeds through the construction of a procapsid, which subsequently undergoes lattice maturation and DNA packaging (*2*, *15*) (Figure 1). The P22 procapsid contains three essential components: 420 molecules of coat protein (gp5, 47 kDa) arranged in a $T = 7$ icosahedral lattice, 200−300 molecules of scaffolding protein (gp8, 34 kDa) contained in the interior, and a dodecameric ring of portal protein (gp1, 87 kDa) located at a singular vertex that forms the site of DNA entry and exit. Scaffolding protein is released at about the time of DNA packaging (*16*). DNA packaging triggers maturation, which results in a 10% increase in the shell diameter (expansion) and concurrent capsid stabilization (*17*, *18*). Maturation is mediated by domain interchange between coat protein subunits and leads to increased stability of subunits and to a small increase in the amount of β-strand secondary structure (*19*−*21*).

The symmetry of the P22 procapsid requires that the coat subunit attain multiple (up to seven) conformations. At least four distinct conformations can be detected by electron cryomicroscopy at intermediate resolution (*18*). In previous biophysical studies, including Raman spectroscopy, conformational changes of the shell subunit during the expansion−maturation step were characterized (*21*−*25*). However, due to technical limitations, it was not possible to obtain spectroscopic signatures of the coat protein monomer and identify the structural changes required for assembly of the procapsid shell. In the study presented here, we employ Raman spectroscopy together with hydrogen/deuterium (H/D) exchange and small-angle X-ray scattering (SAXS) to characterize changes in subunit secondary and tertiary structures with procapsid shell formation. On the basis of these results and the known domain structure of the P22 coat protein (*26*), we propose a mechanism for conformational switching during morphogenesis of the dsDNA viral capsid.

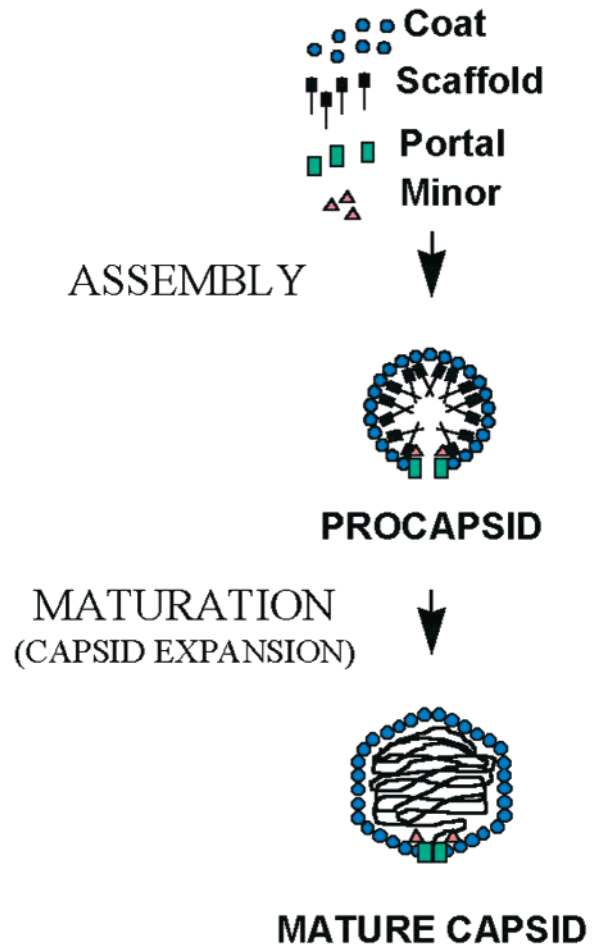

FIGURE 1: Assembly pathway of bacteriophage P22. The co-assembly (top) of 420 copies of coat, 200−300 copies of scaffold, 12 copies of portal, and a few copies of minor proteins yields a procapsid (middle), which matures through DNA packaging, scaffold ejection, and shell expansion to yield a mature capsid (bottom). Subsequent tail attachment is not shown.

MATERIALS AND METHODS

Protein and Procapsid Shell Purifications. Procapsid-like particles composed exclusively of coat and scaffolding proteins were expressed in *Escherichia coli* from a pET-based plasmid (pPM-5-Δ2) that encodes the coat and scaffolding genes (gift from S. Casjens, University of Utah, Salt Lake City, UT). Procapsid purification and scaffolding protein extraction were accomplished using previously described procedures (*27*).

Monomeric coat protein was obtained as follows. Purified procapsids were converted to denatured subunits by treatment with 6 M GuHCl. The denatured subunits were subsequently refolded at a protein concentration of 1 mg/mL by dialysis against buffer B (50 mM Tris, 25 mM NaCl, and 1 mM EDTA) at 4 °C. High-molecular mass aggregates were removed by centrifugation (40 000 rpm, Beckman 40.2 rotor, 2 °C, 2 h). The remaining protein solution was loaded onto a HiTrap-Q ion exchange column (Amersham-Pharmacia-Biotech, Inc., Piscataway, NJ) and eluted with a 0 to 0.3 M NaCl gradient. Aliquots of the peak fraction, which eluted

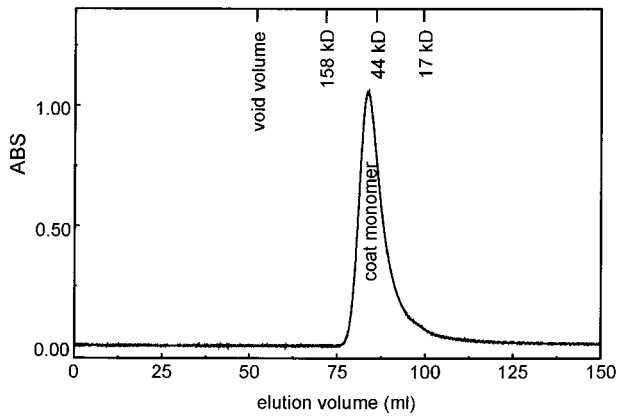

FIGURE 2: Size exclusion chromatography of the concentrated coat protein. Two milliliters of a coat protein solution (16 mg/mL) were loaded onto a TSK 3000 column. The position of the void volume (blue dextran) and elution of molecular mass standards are indicated on the top axis. Monomeric coat eluted in 50 mM Tris and 25 mM NaCl (pH 7.6) as a single peak at 84 mL, indicating an apparent molecular mass of 60 kDa.

at 0.2 M NaCl, were subsequently loaded onto a preparative TSK3000SW (22.5 mm × 300 mm) size exclusion column (TosoHass, Montgomeryville, PA) and eluted with buffer B at a rate of 4 mL/min and 4 °C. In a typical preparation, the Q column-concentrated coat protein was monomeric (Figure 2) and remained monodisperse and assembly active for about 24 h while stored on ice.

Raman Spectroscopy and Hydrogen/Deuterium Exchange. Samples for Raman spectroscopy were prepared from the peak fraction of the Q column. Identical Raman spectra were also obtained on a diluted sample of the protein (1.7 mg/mL) prepared from the monomer peak fraction of the TSK3000SW size exclusion column (Figure 2). Raman spectra were obtained on a Spex 500M single-monochromator spectrograph equipped with a notch filter and charge-coupled device detector (SpectrumOne, Instruments S. A., Edison, NJ). Spectra were excited with 120 mW of the 532 nm line from a solid-state, diode-pumped, frequency-doubled Nd:YVO_4 laser (model Verdi, Coherent, Santa Clara, CA). Samples were thermostated at 2 °C. Hydrogen/deuterium exchange was initiated by rapid buffer exchange [25 mM Tris and 0.2 M NaCl (pD 7.5)] using Biogel P-6 desalting columns (Bio-Rad, Hercules, CA). The exchange was monitored by time-resolved Raman spectroscopy at 2 °C using methods described previously in detail (*28*, *29*).

Small Angle X-ray Scattering. For small-angle X-ray scattering, the coat protein monomer was purified using size exclusion chromatography as described above (the protein concentration of the peak fraction ranging from 0.6 to 1.2 g/L). SAXS data were collected at beam line 4-2 of the Stanford Synchrotron Radiation Laboratory (*30*). The sample was placed in a thin (50 μL, 1.2 mm path) cell with mica windows. The cell was thermostated at 15 °C. Scattered X-rays were detected by use of a one-dimensional position sensitive proportional counter (EMBL/BioLogic model 210). The momentum transfer axis [$Q = 4\pi \sin(\theta)/\lambda$, where 2θ is the scattering angle and λ is the X-ray wavelength (1.38 Å)] of the detector was calibrated using the (100)-reflection of a cholesterol myristate powder sample. X-ray exposures 10 min in duration were subdivided into 10−20 exposures. Individual scattering curves were normalized to the intensity of the incident beam, background-subtracted, and averaged after confirmation of no potential radiation-induced aggregation.

RESULTS AND DISCUSSION

Conformation and Folding of the Coat Protein Subunit

Monomer Shape and Oligomerization. The refolded coat protein subunit eluted as a monomer from the anion exchange column and remained monomeric even at a high concentration (16 g/L) when stored in a buffer containing ≥0.2 M NaCl (Figure 2). The monomer assembled into procapsids when mixed with scaffolding protein in buffer B (data not shown). Compared with globular protein standards, the 47 kDa monomer eluted from a size exclusion column with a higher than expected apparent mass (60 kDa), indicative of an asymmetrically shaped molecule or an expanded (partially unfolded) globular conformation (Figure 2).

To further characterize the compactness and shape of the monomer, SAXS data were collected from dilute solutions (Figure 3). An apparent mass of 49 kDa was obtained by extrapolation of the data of Figure 3A to an angle of 0° using the Guinier approximation (*31*). The SAXS data confirm a monomeric state for the coat protein subunit. The monomer exhibited a radius of gyration of 36.7 ± 0.7 Å, significantly larger than the value of 18.7 Å predicted for a sphere of equivalent volume and mass. The SAXS results thus imply that the monomer is not spherically shaped (*32*).

To gain information about the distribution of mass within the molecule, the reciprocal space data of Figure 3A were transformed into a real space distance distribution function using the regularization method (*33*). The distance distribution function of Figure 3B provides information about the atom-weighted distribution of distances within the molecule. A maximum distance within the protein (D_{max}) of 120 ± 10 Å was obtained, a value considerably larger than expected for a spherical molecule (48 Å). The shape of the monomer was estimated using a simulated annealing procedure and a dummy atom model (*34*). The two best models, shown in Figure 3C, indicate a slightly bent and elongated shape about 100 Å in length.

Secondary Structure. The solution secondary structure of the monomer was probed by Raman spectroscopy using methods similar to those applied previously to the procapsid and capsid shells (*21*, *25*, *29*). The middle trace of Figure 4 shows the Raman spectrum in the region of 600−1800 cm^{-1}. The monomer exhibits a strong and broad amide I band centered near 1667 cm^{-1}, diagnostic of a relatively broad distribution of secondary structures in which β-strand nevertheless predominates (*35*, *36*). A quantitative estimate of the secondary structure distribution using the reference intensity profile method of Berjot et al. (*37*) indicates 22 ± 4% α-helix, 39 ± 2% β-strand, and 38 ± 5% undefined or irregular conformations (loops, turns, coils, and other aperiodic structures). The broad amide III band of the monomer is centered at 1251 cm^{-1}, which is consistent with the amide I profile (*35*, *36*). The Raman-based estimate of 22% α-helix in the monomer is also in agreement with the value of ∼20% α-helix estimated by circular dichroism (CD) (*38*). It should be noted that the significant α-helical content of the coat protein precludes a reliable estimate of β-strand content by

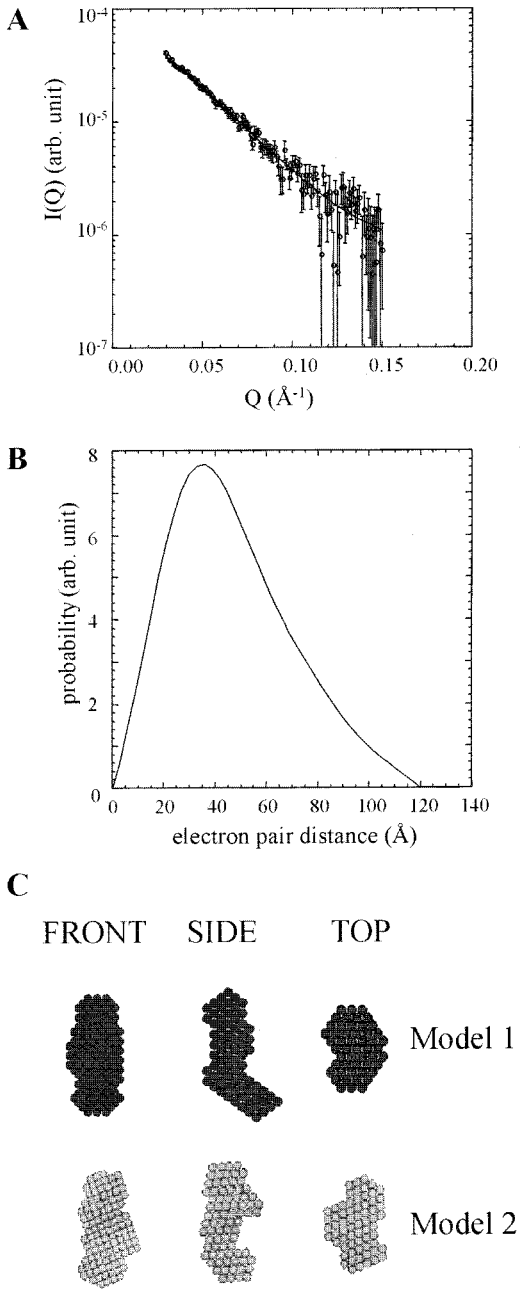

FIGURE 3: Small-angle X-ray scattering of the coat protein monomer. The monomer peak fraction (1.2 g/L) from the TSK 3000 column was used directly to obtain the data. (A) Scattering intensity vs momentum transfer *Q*. (B) The scattering intensity was reproduced by the distance distribution function using an indirect transform method (*32*, *33*). The apparent mass of 49 kDa was obtained by comparison of the intensity extrapolated to zero angle with that of a scaffolding protein standard [covalent dimer (68 kDa) containing the mutation R74C (*70*)]. (C) The two best models for the monomeric subunit are shown in orthogonal projections. The volume for each model is the same as that of the monomer. The models were generated by fitting the data in panel A using the DAMMIN procedure (*34*). A bead diameter of 5 Å was used for fitting and display.

CD spectroscopy. However, Raman spectroscopy clearly identifies β-strand as the prevalent conformation.

The finding of β-strand as the dominant secondary structure in the monomeric state of the coat protein is in accord with Raman results on subunits of the P22 procapsid and capsid shells (*22*, *24*, *25*), and suggests that the fundamental fold is preserved during assembly. Extensive

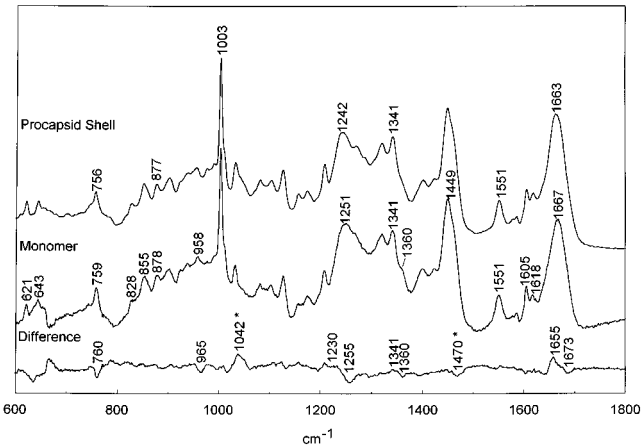

FIGURE 4: Raman spectra in the region of 600−1800 cm^{-1} (532 nm excitation) of the bacteriophage P22 procapsid shell at 18 mg/mL and 10 °C in buffer B (top) and unassembled coat protein monomer at 16 mg/mL and 2 °C in buffer B (middle). The difference spectrum (bottom) was computed by subtraction of the middle spectrum from the top spectrum. Spectra were corrected for Raman scattering of buffer B, and intensities were normalized using the 1003 cm^{-1} band of phenylalanine (*25*).

β-strand structure (in the form of a jellyroll fold) is also prevalent in the capsid subunits of many other icosahedral viruses (*39*−*44*). Recently, the same fold has been demonstrated by Raman spectroscopy for the bacteriophage PRD1 capsid subunit (protein P3, 43 kDa) (*11*). The PRD1 capsid subunit provides a useful comparison for that of P22 because it has been studied extensively by both Raman spectroscopy (*11*) and X-ray crystallography (*39*). On the basis of the Raman amide I profile (*11*), the estimated secondary structure (*37*) for the P3 subunit of the PRD1 capsid is 18% α-helix and 44% β-strand. This is in reasonably good agreement with the X-ray structure of P3, which gives 13% helix and 36% strand (*39*). The modest differences between Raman- and X-ray-determined values of helix and strand presumably reflect overlapping amide I band contributions from other types of structure (turns and irregular conformations) as well as the more strict classification of peptide backbone conformations by X-ray crystallography. Nevertheless, the ratio of β-strand to α-helix is about the same in both X-ray (2.75) and Raman (2.6) analyses. In contrast, a substantially lower β/α ratio (1.8) is obtained for the monomeric subunit of P22, as is apparent from inspection of the corresponding Raman amide I and amide III contours (compare Figure 4 with Figure 3 of ref *11*). The sharper amide I and amide III bands of the PRD1 shell resemble more closely those of the mature P22 shell (*23*). Interestingly, PRD1 is one of the few dsDNA viruses that assembles without an apparent shell maturation (expansion) step; the PRD1 coat protein assembles directly into the mature capsid architecture (*45*).

Finally, we note that the Raman signature of the mature capsid shell of the lambdoid phage HK97 (R. Hendrix, J. M. Benevides, and G. J. Thomas, Jr., unpublished data) exhibits clearly discernible α-helix markers, viz. an amide I shoulder at 1654 cm^{-1} and enhanced amide III intensity between 1250 and 1300 cm^{-1}, consistent with the recently determined X-ray crystal structure (*46*). Thus, despite the similar icosahedral capsid architectures of PRD1, P22, and HK97, significantly different subunit folds are evident from the respective Raman amide band signatures. The protein

folds of P22 and PRD1 subunits have more in common with one another than with that of HK97 (*46*).

Tertiary Structure. In addition to the assessment of secondary structure, Raman spectroscopy permits evaluation of tertiary structure through a variety of conformation- and environment-sensitive marker bands of selected side chains. Several of these marker bands are discussed next.

Raman indicators of the average hydrogen-bonding environment of the eight tyrosine phenolic groups of coat protein occur at 828 and 855 cm^{-1}. In the monomer spectrum (Figure 4, middle trace), these bands exhibit an intensity ratio (I_{855}/I_{828}) of ≈2. This is close to the maximum value of 2.5, which is diagnostic of a phenoxyl group that acts exclusively as the acceptor of a hydrogen bond (*47*). Accordingly, in the monomeric state, the majority of the eight tyrosines per coat protein subunit have the phenolic oxygen engaged as a hydrogen-bond acceptor. [The low intensity of the 828 cm^{-1} band can also arise from a tyrosine phenoxyl that is not hydrogen bonded, as occurs, for example, in the protein coat of Ff filamentous virus or in the vapor phase of *p*-cresol (*48*−*50*). However, such a condition is not expected for tyrosines of globular proteins or their assemblies.]

The relatively intense 760 cm^{-1} band of tryptophan (normal mode *W18*) suggests that the average environment of the six tryptophans per subunit is relatively polar (*51*). The *W17* mode of Trp, which is sensitive to hydrogen bonding of the indolyl N1H group, is observed at 880 cm^{-1}. This is consistent with relatively weak hydrogen bonding (*52*). The distinct shoulder at 1360 cm^{-1} is part of a tryptophan Fermi doublet [1340/1360 cm^{-1} (*53*)] that is sensitive to the hydrophobicity of the indolyl ring environment. Its intensity in the P22 shell monomer is similar to that observed for the small globular protein, *E. coli* thioredoxin (*54*), which contains two partially exposed Trp residues. Thus, the tryptophan residues of the coat protein are considered to be at least partially exposed to solvent in the monomeric state.

The tryptophan marker at 1551 cm^{-1} is assigned to the indolyl *W3* mode, the wavenumber value of which is diagnostic of the magnitude of the side chain torsion angle $\chi^{2,1}$ (*55*). The data presented here indicate that the average C3−Cβ bond has a $|\chi^{2,1}|$ of ≈95°. The position and sharpness of this marker suggest further that all indolyl rings adopt the same $|\chi^{2,1}|$ value. In previous work, a single-exponential decay of tryptophan fluorescence was reported for the coat protein monomer, implying that the six Trp residues per subunit share a similar amphipathic local environment (*56*). The results presented here are consistent with the fluorescence data and show further that all Trp side chain orientations are virtually identical with respect to $|\chi^{2,1}|$.

The Raman band corresponding to the sulfhydryl (S−H) stretching vibration of cysteine is diagnostic of the hydrogen-bonding environment of the S−H group (*57*). For the single cysteine (Cys 405) of the coat protein monomer, the Raman marker is observed at 2568 cm^{-1}, which indicates that the S−H group is the donor of a moderately strong hydrogen bond. The sharpness of the band further indicates that the S−H···X hydrogen bond adopts a single, well-defined configuration; e.g., there is no heterogeneity among different monomer molecules (*21*, *57*). Thus, the C-terminal domain attains the same well-defined tertiary structure in all subunits in solution.

Conformational Changes with Procapsid Assembly

To characterize structural changes accompanying subunit assembly, we compared Raman signatures of the monomeric subunit and the procapsid shell. The icosahedral procapsid shell ($T = 7$), which is composed solely of the coat protein subunit (gp5), is generated by selective removal of scaffolding and minor proteins using low concentrations of GuHCl. Despite subtle alterations in capsid morphology attendant with GuHCl treatment (*58*), previous studies have demonstrated that Raman spectra of GuHCl-treated and untreated shells are identical, provided that the spectral contribution from the scaffolding protein is compensated (*25*). These experiments demonstrate that GuHCl treatment does not appreciably alter the subunit conformation.

Secondary Structure. Although Raman spectra of the monomeric and procapsid shell states of coat protein share many similar features, it is clear from Figure 4 that procapsid assembly perturbs the structure of the coat protein monomer. The computed difference spectrum shown in the bottom trace of Figure 4 highlights the spectral changes accompanying assembly.

Importantly, the center of the Raman amide I marker is shifted from 1667 cm^{-1} in the monomer to 1663 cm^{-1} in the procapsid shell. This shift gives rise to Raman difference peaks at 1655 cm^{-1} (assigned to α-helix) and 1673 cm^{-1} (β-strand) and corresponding troughs at lower and higher wavenumber values. The difference band pattern of Figure 4 reflects a narrower amide I profile in the procapsid shell spectrum; i.e., the more ordered secondary structure of the shell subunit occurs at the expense of disordered chain segments (loops, coil, etc.) in the monomer. The more highly ordered secondary structure of the subunit in the assembled shell is further demonstrated in the difference spectrum of Figure 4 by the diminished intensity of the Raman amide III band at 1255 cm^{-1}, assigned to disordered structure (*25*, *36*, *59*) and enhanced intensity of the Raman amide III marker at 1230 cm^{-1} (β-strand). Despite overlapping contributions expected from various side chains near 900−1000 and 1300−1350 cm^{-1} (*53*, *60*), we may interpret the negative difference band at 965 cm^{-1} (*61*) and positive difference band at 1341 cm^{-1} (*62*) also as indications of a more highly α-helical secondary structure in subunits of the procapsid shell.

Overall, it is clear from Figure 4 that the polypeptide backbone of the coat protein monomer undergoes refolding during procapsid assembly. An estimate of the number of peptide linkages involved can be obtained from the normalized area of the amide I band differences. We obtain 4 ± 1% of the backbone, or 17 of 428 peptide bonds. In a recent study, Lanman and co-workers (*26*) demonstrated that a flexible hinge encompassing residues 180−205 of the subunit becomes protease-resistant upon procapsid assembly. Residues within this hinge are likely candidates for refolding. Thus, assembly of the P22 procapsid leads to local ordering of a small but significant percentage of the peptide residues. Similar subunit folding has been reported for capsid assembly of the P3 subunit of PRD1 (*11*). In the case of PRD1, however, a smaller subset (∼2%) of peptide linkages is involved. Also, the PRD1 capsomeres (P3 trimers) do not exhibit the assembly-induced increase in global stability (*11*) that characterizes subunits of the P22 shell lattice (*26*, *63*).

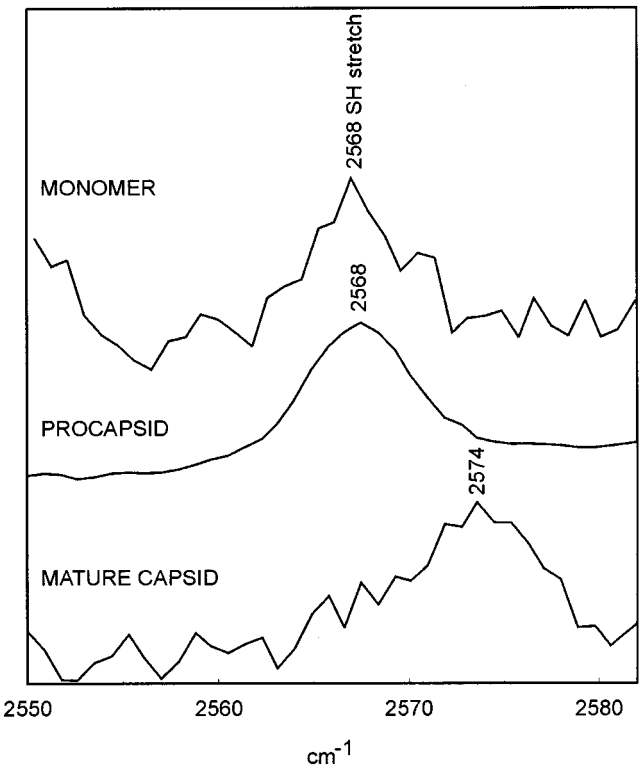

FIGURE 5: Raman spectra in the region of 2550−2580 cm^{-1} (532 nm excitation) of the P22 coat protein monomer (top), procapsid shell (middle), and mature capsid shell (bottom). Monomer and shell concentrations and other conditions are as given in the legend of Figure 4. Mature shells were prepared as previously described (*21*).

Tertiary Structure. In addition to the changes in subunit secondary structure noted above, P22 procapsid assembly leads to changes in tertiary structure that are also revealed by Raman spectroscopy. The shift of the tryptophan *W18* marker from 760 cm^{-1} in the monomer to 756 cm^{-1} in the procapsid shell with a concomitant large decrease in intensity (Figure 4) signifies a substantial change in the amphipathic environment of the average Trp side chain. Broadening of the 1360 cm^{-1} component of the Trp Fermi doublet indicates that this change is due to a more hydrophilic indolyl environment in the procapsid shell subunit.

The tryptophan *W3* marker (1551 cm^{-1}) exhibits no assembly-related shift in its band center, indicating a negligible change in the average $|\chi^{2,1}|$ torsion (*55*). Overall, Raman spectral features diagnostic of the Trp side chains exhibit only very small changes with the transition from the monomer to procapsid shell. This contrasts dramatically with the large Trp side chain reorientations that accompany shell expansion (*22*).

Invariant to the assembly process are Raman indicators of hydrogen bonding by tyrosine phenoxyls (markers at 830 and 850 cm^{-1}, Figure 4) and by the cysteine sulfhydryl of Cys 405 (marker at 2568 cm^{-1}, Figure 5). Additionally, other assigned Raman markers of the aliphatic and aromatic side chains of coat protein (*22*−*24*) are affected little by assembly of the procapsid (Figure 4). Thus, despite measurable folding of the coat protein backbone upon procapsid assembly, the tertiary structure of the subunit is not significantly affected. In this regard, the P22 shell assembly is similar to that of PRD1 (*11*).

It is interesting to note, however, that in contrast to the formation of the P22 procapsid shell from monomers, the process of shell maturation (procapsid-to-capsid transformation) leads to large and extensive changes in both the environments and hydrogen-bonding interactions of numerous side chains (*21*, *22*). A striking example of this effect, which is illustrated in Figure 5, is the large wavenumber shift (2568 → 2574 cm^{-1}) that occurs in the Raman S−H marker of Cys 405 with shell maturation. Clearly, the moderate S−H···X hydrogen bond of the Cys 405 sulfhydryl in the monomer is replaced by a much weaker hydrogen bond in the subunit of the mature capsid (*21*, *57*). [See also the discussion of SH → SD exchange dynamics of the monomer and shells (below).] Because of the location of Cys 405 near the C-terminus of the subunit sequence, it is concluded that the C-terminal domain, and particularly the local environment of the Cys 405 sulfhydryl group, plays a key role in monomer folding and capsid maturation processes, but not in the procapsid assembly step.

Hydrogen/Deuterium Exchange Dynamics

Amide Exchange. In previous work, we compared the Raman signatures and the rates of deuterium exchange of amide NH groups (H/D exchange) in subunits of the P22 procapsid and capsid (*21*). The data revealed that although the procapsid-to-capsid maturation occurs with conservation of subunit secondary structure (*22*), it is accompanied by a very large (2-fold) increase in the level of exchange protection of shell subunits, as well as the above-noted extensive changes in side chain environments (*22*). These results indicate that the shell transformation involves subunit domain movement accompanied by a large increase in the level of effective exchange protection in the core of the subunit, without appreciable refolding of subunit domains. Here, we extend the previous approaches (*21*, *28*) and employ Raman amide bands to compare H/D exchange dynamics of the monomer and procapsid shell subunit. H/D exchange was previously probed both at low temperatures (exchange via the native conformation) and at elevated temperatures (exchange via a locally unfolded conformation). However, because the monomer is intrinsically less thermostable than the shell assembly and subject to off-pathway aggregation at elevated temperatures, this study has been limited to exchange under strictly native conditions.

Figure 6A compares Raman markers in the amide I region of the monomer and procapsid shell subunit, following exposure of each sample to D_2O (pD 7.8) under native conditions (2 °C for the monomer and 10 °C for the procapsid shell). As expected, the band centers are shifted by deuteration to wavenumber values lower (amide I′) than those that occur in the corresponding nondeuterated samples (cf. amide I markers of Figure 4). Deuterium exchange was allowed to reach a plateau, about 30 min for the monomer and 120 min for the procapsid shell, after which further exchange was negligible. However, not all amide NH sites become deuterated under these native conditions (see also amide III′ markers in Figure 6C). The dominant Raman band in each spectrum of Figure 6A actually represents an overlap of contributions from amide I′ (due to exchanged ND peptides) and amide I (due to residual nonexchanged NH peptides). The composite amide I/amide I′ band of the monomer is centered at 1658 cm^{-1}, while that of the

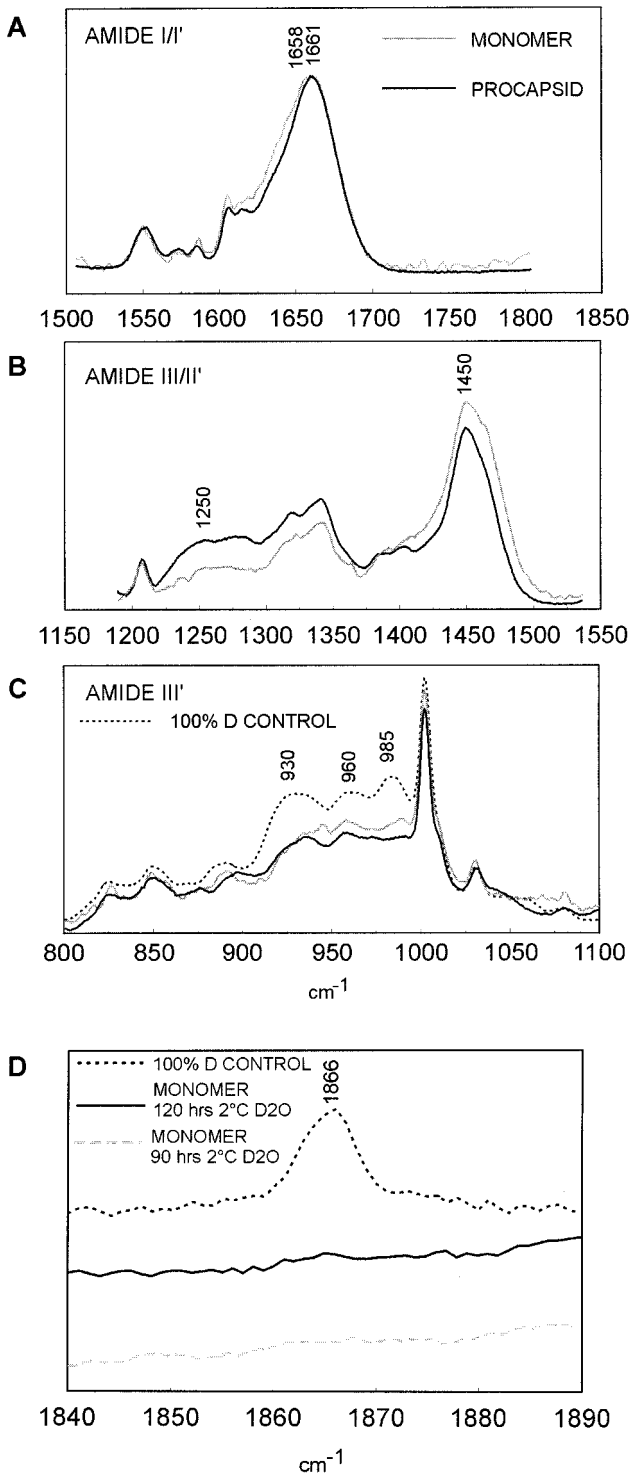

FIGURE 6: Normalized Raman signatures of native-state H/D exchanges of the P22 coat protein monomer (2 °C) and procapsid shell (10 °C), following exposure to D_2O buffer for 12 h (see the text): (A) amide I/amide I′ profiles, (B) amide III/amide II′ profiles, (C) amide III′ profiles, and (D) S−D stretching band profiles, following prolonged exposure to D_2O. Included in panel D as a control is the S−D band profile of the fully exchanged procapsid subunit incubated at 40 °C (see the text).

procapsid shell is centered at 1661 cm^{-1}. The lower wavenumber value for the composite band of the monomer reflects both a slightly different secondary structure and a greater degree of amide H/D exchange vis-à-vis the subunit of the procapsid shell. (By comparison, the nonexchanged monomer and procapsid shell subunit yield amide I bands centered at 1664 and 1667 cm^{-1}, respectively, as seen in Figure 4.)

The corresponding Raman amide III profile (due to nonexchanged NH groups) and amide II′ profile (due to exchanged ND groups), shown in Figure 6B, are entirely consistent with the amide I/amide I′ data depicted in Figure 6A. Thus, the monomer exhibits a lower amide III intensity (∼1250 cm^{-1}) and a greater amide II′ intensity (∼1450 cm^{-1}) than the procapsid shell subunits, owing to more extensive native-state H/D exchange in the monomer.

Figure 6C compares Raman profiles in the amide III′ region (900−1000 cm^{-1}, due to exchanged ND groups) of the monomer and procapsid shell subunit after native-state exchange. Also shown in Figure 6C is the amide III′ profile of a coat protein control in which all NH groups have been exchanged with deuterium under denaturing conditions prior to refolding of the protein in D_2O. Again, these data confirm that H/D exchange is more extensive in the monomer than in the procapsid shell subunits. In particular, greater amide III′ intensity is observed at 930−945 cm^{-1} which can be assigned to deuterated α-helix (*62*, *64*), at 960 cm^{-1} which can be assigned to deuterated disordered peptides (*21*, *35*, *36*), and at 980−990 cm^{-1} which can be assigned to deuterated *β*-strand (*21*, *35*, *36*, *64*). The amide III′ exchange profile of the monomer indicates that the protein fold of the monomer comprises unprotected and protected residues in regions of α-helical, *β*-stranded, and disordered secondary structure. Panels B and C of Figure 6 also show that neither the procapsid shell subunit nor the monomer undergoes complete exchange of all peptide residues located in α-helical, *β*-stranded, or disordered regions of secondary structure. The data suggest that the most protected residues of the monomer are those located in regions of *β*-strand structure.

The substantial exchange protection of the monomer, estimated from Figure 6C as 30% of all NH sites, indicates that the protein fold is sufficiently well defined to produce a relatively compact tertiary structure. Accordingly, the less compact and "molten-globule-like" segments of the protein implied by binding of the hydrophobic probe bis-ANS (*38*) may be limited to small regions localized at the protein surface and potentially involved in shell assembly. One locus of the monomer that is likely to undergo a folding-like conformational change upon assembly is the interdomain hinge region (residues 180−205), which becomes more protease-resistant and exchange-protected in the procapsid shell (R. Tuma and P. E. Prevelige, manuscript submitted for publication) (*26*).

Side Chain Exchange. H/D exchange of selected side chains can be used to localize and monitor the folding core of a protein (*11*, *21*, *25*, *28*, *46*). For example, the single sulfhydryl of the coat protein (Cys 405) provides a selective probe of exchange of the C-terminal region. Figure 6D shows Raman spectra in the region of 1840−1890 cm^{-1}, where the stretching vibration of the deuterated sulfhydryl group (S−D) is expected to occur. The absence of an S−D band in the spectrum of the monomer shows unequivocally that the Cys 405 sulfhydryl is fully protected against H/D exchange. Protection persists for samples incubated under native conditions (pD 7.8 and 2 °C) for up to 6 days. The SH group can be exchanged only under conditions that favor global unfolding (40 °C). Thus, the Cys 405 sulfhydryl is buried within the hydrophobic folding core of the monomer. A

similar degree of sulfhydryl exchange protection is observed for the procapsid shell subunit (*21*).

The hydrogen-bonding state of the Cys 405 sulfhydryl is also similar in the monomer and procapsid shell subunit [cf. Figure 5 and the data of Tuma at al. (*21*)]. However, both the hydrogen-bonding environment and exchange protection of the sulfhydryl are dramatically altered in the mature capsid, where S−H···X hydrogen bonding is considerably weaker (*21*). Shell expansion and SH → SD exchange of the procapsid subunit have been shown to be governed by similar activation energies (*21*). This finding strongly suggests that shell maturation is mediated by a structural rearrangement at the locus of Cys 405 (exchange-protected folding core), consistent with a mechanism involving an interchange of subunit domains (*21*). Therefore, it is reasonable to conclude that S−H···X hydrogen bonding of the Cys 405 sulfhydryl provides an important source of stabilization of the monomer in a coupled folding−assembly process.

CONCLUSIONS

A biological requirement of the unassembled coat protein monomer of P22 is a well-defined tertiary structure, which can support the specific biomolecular recognition required for shell assembly without compromising the flexibility that is essential for quasi-equivalent contacts in a $T = 7$ icosahedron. This study demonstrates that this requirement is met by an elongated molecule containing much of the β-strand secondary structure also present in the subunit of the mature capsid assembly. Nevertheless, subtle structural alterations are shown to take place between monomeric and assembled states of the subunit.

In particular, approximately 17 of the 430 amino acid residues undergo a refolding event in which they become assimilated as regions of α-helix and β-strand secondary structure. These residues may correspond to the flexible linker region recently identified in studies of proteolytic susceptibility (*26*). A similar linker region has been identified in the FG loop of bacteriophage MS2 coat protein, which also adopts multiple conformations along the assembly pathway (*13*, *14*). Another example of such refolding is the selective formation of a β-strand annulus at the pseudo-3-fold axis in the capsid of the single-stranded RNA plant virus CCMV (*40*).

Previous H/D exchange studies revealed that the procapsid shell subunit retains a considerable degree of conformational flexibility, and that this degree of freedom is lost during the subsequent expansion−maturation step (*21*). On the basis of this finding, it was suggested that the subunit within the procapsid resembles a late folding intermediate. Present results show that assembly of the monomer into the procapsid shell has surprisingly little effect on the environments of subunit side chains. There is essentially no change in tyrosine and cysteine hydrogen-bonding environments and, at most, a very small change in the average indolyl hydrophobicity of tryptophan. In addition, both H/D exchange and SAXS measurements indicate that the unassembled subunit adopts a relatively compact tertiary structure. Therefore, the coat protein monomer represents a compact, late-folding intermediate that is only slightly more locally disordered than its procapsid shell counterpart.

The interrelationship between folding and assembly can be depicted in the context of an energy landscape, as shown in Figure 7. At high dilutions, the coat protein folds into a soluble monomer and, apart from a flexible loop (∼20 residues) of the polypeptide chain, adopts secondary and tertiary structures similar to those of the subunit incorporated within the procapsid shell. At higher concentrations (>1 mg/mL; R. Tuma, H. Tsuruta, and P. E. Prevelige, Jr., unpublished data), the monomer gradually overcomes the high entropic barrier, generated in part by ordering of the loop region, and assembles (*65*, *66*). The activation barrier is presumed to be lowered by the presence of the scaffolding protein, which acts as an entropy sink by utilizing the energy of scaffolding protein dimerization to promote coat subunit association (*67*, *70*). Thus, the disorder−order transition within the loop region is thermodynamically coupled to the binding of the scaffolding protein and in effect exerts control over the assembly process.

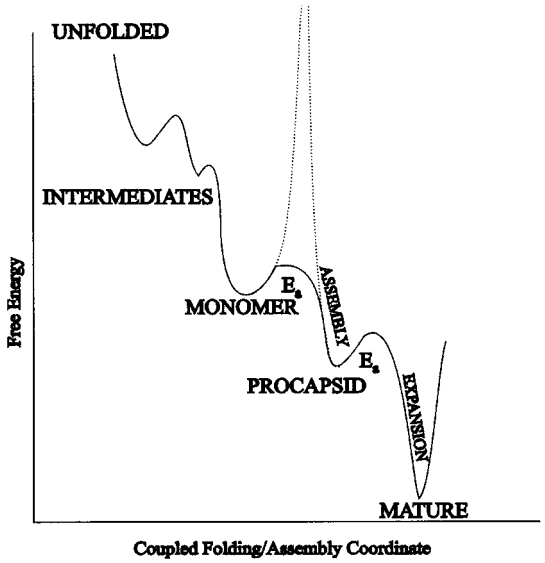

FIGURE 7: Schematic energy landscape for folding and assembly of P22 coat protein. The broader minima for the monomer and procapsid subunit indicate greater conformational flexibility of these states. The height of the free energy barrier separating the monomer and procapsid states is lowered in the presence of the scaffolding protein. The sharp and deep minimum for the mature subunit reflects its greater dynamic stability as revealed by hydrogen isotope exchange. The energy landscape that the monomer experiences at infinite dilution is shown by a dotted line. In this case, the procapsid state is separated from the monomeric state by an infinitely high free energy barrier.

Both the monomeric coat protein and the coat protein subunits within the procapsid retain a considerable degree of conformational freedom, a phenomenon typical of (late) folding intermediates (*68*). It has been pointed out that viral capsids are faced with the conflicting demands of achieving fidelity during assembly and stability of the final structure, and that these demands can be met through the use of many weak interactions (*69*). Although providing sufficient energy to form a stable precursor capsid, such weak interactions might be insufficient to form extremely stable viral capsids. A general scheme for circumventing this problem is a two-step assembly process in which a metastable precursor form is subsequently stabilized. In the case of phage HK97, such stabilization is achieved through extensive covalent cross-linking, whereas in certain other cases (e.g., adenovirus and herpesvirus), it is achieved through the use of "glue" proteins. However, in P22 and many other dsDNA viruses, a procapsid

with weak subunit−subunit contacts is assembled initially, and then is converted into a capsid with much stronger intersubunit interactions. This maturation process, which is encoded within the primary sequence of the coat protein, is accomplished via a shift in the energy landscape of the subunit within the procapsid lattice. On this landscape, a new low-energy state, corresponding to the mature capsid, becomes accessible. This state is populated after expansion. During expansion, the subunit secondary structure is perturbed only modestly (2−3% increase in β-strand content), but the tertiary structure is radically altered (domain rearrangements), and the exchange-protected folding core that is common to both the procapsid-assembled subunit and the monomer undergoes a major (2-fold) increase in its level of protection. These findings, which for the first time include studies of the coat protein monomer, extend and confirm the previously proposed two-step folding model for the P22 coat protein (*21*).

REFERENCES

1. Rossmann, M. G. (1984) *Virology 134*, 1−11.
2. King, J., and Chiu, W. (1997) in *Structural Biology of Viruses* (Chiu, W., Burnett, R. M., and Garcea, R., Eds.) pp 288−311, Oxford University Press, New York.
3. Canady, M. A., Tihova, M., Hanzlik, T. N., Johnson, J. E., and Yeager, M. (2000) *J. Mol. Biol. 299*, 573−584.
4. Zlotnick, A., Reddy, V. S., Dasgupta, R., Schneemann, A., Ray, W. J., Jr., Rueckert, R. R., and Johnson, J. E. (1994) *J. Biol. Chem. 269*, 13680−13684.
5. Chow, M., Basavappa, R., and Hogle, J. M. (1997) in *Structural Biology of Viruses* (Chiu, W., Burnett, R. M., and Garcea, R., Eds.) pp 157−186, Oxford University Press, New York.
6. Wien, M. W., Chow, M., and Hogle, J. M. (1996) *Structure 4*, 763−767.
7. Belnap, D. M., Filman, D. J., Trus, B. L., Cheng, N., Booy, F. P., Conway, J. F., Curry, S., Hiremath, C. N., Tsang, S. K., Steven, A. C., and Hogle, J. M. (2000) *J. Virol. 74*, 1342−1354.
8. Tsang, S. K., Danthi, P., Chow, M., and Hogle, J. M. (2000) *J. Mol. Biol. 296*, 335−340.
9. Rossmann, M. G., and Erickson, J. W. (1985) in *Virus Structure and Assembly* (Casjens, S., Ed.) pp 30−73, Jones and Bartlett, Boston.
10. Duda, R. L., Martincic, K., and Hendrix, R. W. (1995) *J. Mol. Biol. 247*, 636−647.
11. Tuma, R., Bamford, J. H. K., Bamford, D. H., Russell, M. P., and Thomas, G. J., Jr. (1996) *J. Mol. Biol. 257*, 87−101.
12. Kumar, S., Ma, B., Tsai, C. J., Sinha, N., and Nussinov, R. (2000) *Protein Sci. 9*, 10−19.
13. Golmohammadi, R., Valegard, K., Fridborg, K., and Liljas, L. (1993) *J. Mol. Biol. 234*, 620−639.
14. Ni, C. Z., Syed, R., Kodandapani, R., Wickersham, J., Peabody, D. S., and Ely, K. R. (1995) *Structure 3*, 255−263.
15. Casjens, S., and Hendrix, R. (1988) in *The Bacteriophages* (Calendar, R., Ed.) pp 15−91, Plenum Press, New York.
16. King, J., and Casjens, S. (1974) *Nature 251*, 112−119.
17. Earnshaw, W., Casjens, S., and Harrison, S. C. (1976) *J. Mol. Biol. 104*, 387−410.
18. Prasad, B. V., Prevelige, P. E., Marietta, E., Chen, R. O., Thomas, D., King, J., and Chiu, W. (1993) *J. Mol. Biol. 231*, 65−74.
19. Galisteo, M. L., and King, J. (1993) *Biophys. J. 65*, 227−235.
20. Prevelige, P. E., Jr., and King, J. (1993) *Prog. Med. Virol. 40*, 206−221.
21. Tuma, R., Prevelige, P. E., Jr., and Thomas, G. J., Jr. (1998) *Proc. Natl. Acad. Sci. U.S.A. 95*, 9885−9890.
22. Prevelige, P. E., Jr., Thomas, D., Aubrey, K. L., Towse, S. A., and Thomas, G. J., Jr. (1993) *Biochemistry 32*, 537−543.
23. Prevelige, P. E., Jr., Thomas, D., King, J., Towse, S. A., and Thomas, G. J., Jr. (1990) *Biochemistry 29*, 5626−5633.
24. Thomas, G. J., Jr., Li, Y., Fuller, M. T., and King, J. (1982) *Biochemistry 21*, 3866−3878.
25. Tuma, R., Prevelige, P. E., Jr., and Thomas, G. J., Jr. (1996) *Biochemistry 35*, 4619−4627.
26. Lanman, J. K., Tuma, R., and Prevelige, P. E., Jr. (1999) *Biochemistry 38*, 14614−14623.
27. Prevelige, P. E., Jr., Thomas, D., and King, J. (1993) *Biophys. J. 64*, 824−835.
28. Tuma, R., and Thomas, G. J., Jr. (1996) *Biophys. J. 71*, 3454−3466.
29. Tuma, R., and Thomas, G. J., Jr. (1997) *Biophys. Chem. 68*, 17−31.
30. Tsuruta, H., Brennan, S., Rek, Z. U., Irving, T. C., Tompkins, W. H., and Hodgson, K. O. (1998) *J. Appl. Crystallogr. 31*, 672−682.
31. Serdyuk, I. N., Tsalkova, T. N., Svergun, D. I., and Izotova, T. D. (1987) *J. Mol. Biol. 194*, 126−128.
32. Feigin, L. A., and Svergun, D. I. (1987) *Structure Analysis by Small-Angle X-ray and Neutron Scattering*, Plenum Press, New York.
33. Svergun, D. I. (1991) *J. Appl. Crystallogr. 24*, 485−492.
34. Svergun, D. I. (1999) *Biophys. J. 76*, 2879−2886.
35. Chen, M. C., and Lord, R. C. (1974) *J. Am. Chem. Soc. 96*, 4750−4752.
36. Chen, M. C., Lord, R. C., and Mendelsohn, R. (1974) *J. Am. Chem. Soc. 96*, 3038−3042.
37. Berjot, M., Marx, J., and Alix, A. J. P. (1987) *J. Raman Spectrosc. 18*, 289−300.
38. Teschke, C. M., King, J., and Prevelige, P. E., Jr. (1993) *Biochemistry 32*, 10658−10665.
39. Benson, S. D., Bamford, J. K., Bamford, D. H., and Burnett, R. M. (1999) *Cell 98*, 825−833.
40. Speir, J. A., Munshi, S., Wang, G., Baker, T. S., and Johnson, J. E. (1995) *Structure 3*, 63−78.
41. Rossmann, M. G., and Johnson, J. E. (1989) *Annu. Rev. Biochem. 58*, 533−573.
42. Hartman, K. A., McDonald-Ordzie, P. E., Kaper, J. M., Prescott, B., and Thomas, G. J., Jr. (1978) *Biochemistry 17*, 2118−2123.
43. Verduin, B. J., Prescott, B., and Thomas, G. J., Jr. (1984) *Biochemistry 23*, 4301−4308.
44. Li, T., Chen, Z., Johnson, J. E., and Thomas, G. J., Jr. (1992) *Biochemistry 31*, 6673−6682.
45. Butcher, S. J., Bamford, D. H., and Fuller, S. D. (1996) *EMBO J. 14*, 6078−6086.
46. Wikoff, W. R., Liljas, L., Duda, R. L., Tsuruta, H., Hendrix, R. W., and Johnson, J. E. (2000) *Science 289*, 2129−2133.
47. Siamwiza, M. N., Lord, R. C., Chen, M. C., Takamatsu, T., Harada, I., Matsuura, H., and Shimanouchi, T. (1975) *Biochemistry 14*, 4870−4876.
48. Overman, S., and Thomas, G. J., Jr. (1995) *Biochemistry 34*, 5440−5451.
49. Overman, S., and Thomas, G. J., Jr. (1998) *J. Raman Spectrosc. 29*, 23−29.
50. Arp, Z., Laane, J., Overman, S. A., and Thomas, G. J., Jr. (2001) *Biochemistry 40* (in press).
51. Miura, T., Takeuchi, H., and Harada, I. (1991) *Biochemistry 30*, 6074−6080.
52. Takeuchi, H., and Harada, I. (1986) *Spectrochim. Acta 42A*, 1069−1078.
53. Harada, I., Miura, T., and Takeuchi, H. (1986) *Spectrochim. Acta 42A*, 307−312.
54. Li, H., Hanson, C., Fuchs, J. A., Woodward, C., and Thomas, G. J., Jr. (1993) *Biochemistry 32*, 5800−5808.
55. Miura, T., Takeuchi, H., and Harada, I. (1989) *J. Raman Spectrosc. 20*, 667−671.
56. Prevelige, P. E., Jr., King, J., and Silva, J. L. (1994) *Biophys. J. 66*, 1631−1641.
57. Li, H., and Thomas, G. J., Jr. (1991) *J. Am. Chem. Soc. 113*, 456−462.

58. Thuman-Commike, P. A., Greene, B., Jakana, J., McGough, A., Prevelige, P. E., and Chiu, W. (2000) *J. Virol. 74*, 3871−3873.
59. Tuma, R., Parker, M. H., Weigele, P., Sampson, L., Sun, Y., Krishna, N. R., Casjens, S., Thomas, G. J., Jr., and Prevelige, P. E., Jr. (1998) *J. Mol. Biol. 281*, 81−94.
60. Overman, S. A., and Thomas, G. J., Jr. (1999) *Biochemistry 38*, 4018−4027.
61. Krimm, S. (1987) in *Biological applications of Raman spectroscopy* (Spiro, T. G., Ed.) pp 1−45, Wiley-Interscience, New York.
62. Overman, S. A., and Thomas, G. J., Jr. (1998) *Biochemistry 37*, 5654−5665.
63. Galisteo, M. L., Gordon, C. L., and King, J. (1995) *J. Biol. Chem. 270*, 16595−165601.
64. Yu, T.-J., Lippert, J. L., and Peticolas, W. L. (1973) *Biopolymers 12*, 2161−2176.
65. Earnshaw, W., and King, J. (1978) *J. Mol. Biol. 126*, 721−747.
66. Casjens, S., and King, J. (1974) *J. Supramol. Struct. 2*, 202−224.
67. Thuman-Commike, P. A., Greene, B., Jakana, J., Prasad, B. V., King, J., Prevelige, P. E., Jr., and Chiu, W. (1996) *J. Mol. Biol. 260*, 85−98.
68. Kamtekar, S., Schiffer, J. M., Xiong, H., Babik, J. M., and Hecht, M. H. (1993) *Science 262*, 1680−1685.
69. Burnett, R. M. (1985) *J. Mol. Biol. 185*, 125−143.
70. Parker, M. H., Stafford, W. F., III, and Prevelige, P. E., Jr. (1997) *J. Mol. Biol. 268*, 655−665.

BI001965Y